Chapter 2

Synthesis and Characterization of Silver Nanoparticles with Varying Physico-chemical Properties

Part of the work presented in this chapter has been published as per the following details: Fageria, L, Pareek, V. et al. (2017) *ACS Omega* 2: 1489-1504.

2.1 Introduction

Silver has a very rich history of its use as an antimicrobial agent. Use of silver in clinical field has been stepped by Dr. J. Marion Sims, who used silver for the treatment of vesico-vaginal fistulas in the year 1852 (Alexander, 2009). Owing to the antibacterial property of silver, its vessels have been utilized for the preservations of perishable items as well as for disinfection of water since long back. The significant increase of MDR microorganisms in the recent years leads scientists to re-exploit the various silver species as possible antimicrobial agents. Over the last few decades, Ag NPs has attracted much interest in the scientific community because of their knowingly innovative and improved physical, chemical and biological properties attributed to their varying physico-chemical properties viz. variation in size, shape, surface capping and synthesis methods (Ivask et al., 2013; Fageria et al., 2017; Pareek et al., 2018). Silver nanoparticles (Ag NPs) are presently used as an antimicrobial agent in wound dressings, textiles, food storage containers, and personal care appliances. It has been reported that the antibacterial properties of Ag NPs depends on their physico-chemical properties (Morones et al., 2005). As far as shape is concerned, spherical shaped NPs are considered best for various applications (Agnihotri et al., 2014).

This chapter deals with the synthesis of Ag NPs with variation in their physico-chemical properties viz. variation in size and surface capping using chemical and biological synthesis methods. As discussed in chapter 1, bottom-up approaches in which atoms or molecules are assembled gradually to construct NPs, are known to be best for the synthesis of NPs because of their potential to synthesize homogenous nanostructures with perfect crystallographic and surface structures. In addition, the synthesized NPs own higher stability, which enhances their antibacterial activity. A variety of bottom-up approaches have been developed for the synthesis of NPs, of which chemical reduction method and fungus mediated biological synthesis methods were utilized in the present study.

2.2 Chemical reduction method

Chemical reduction of metal ions is the most commonly employed method for the synthesis of metal NPs in solutions. This method stands as a first choice for the synthesis of noble metal NPs and involves reduction of an ionic salt using particular reducing agent(s) in an appropriate medium in presence of stabilizing agent(s) (Mishra et al., 2014; Bhargava et al., 2018). An array of reducing agents such as hydrogen, hydrazine, alcohols, carbon monoxide, sodium borohydride, trisodium citrate, etc. have been used to prepare metal

colloids in the nanometer size range (Schmid and Chi, 1998; Evanoff Jr and Chumanov, 2005). Use of strong reducing agents such as sodium borohydride results in the formation of small sized NPs whereas, use of weak reducing agents such as trisodium citrate results in the formation of relatively large NPs (Agnihotri et al., 2014).

2.2.1 Materials

Silver nitrate (>99.9% pure), sodium borohydride ($NaBH_4$, >99%pure), trisodium citrate (TSC, >99% pure), and sodium hydroxide were purchased from Merck (India). 3-mercaptopropionic acid, lysozyme (chicken egg white) and L-fucose were purchased from Sigma-Aldrich (USA). Milli-Q water was acquired from a Milli-Q Biocel water purification system manufactured by Merck Millipore (Merck KGaA, Darmstadt, Germany).

2.2.2 Synthesis of Ag NPs with variation in size and surface capping

Ag NPs with varying sizes were synthesized following the protocol of Agnihotri et al. (2014). In this method, sodium borohydride ($NaBH_4$) and trisodium citrate (TSC) were used as a primary and secondary reducing agent, respectively. TSC has a dual role in this reaction as it functions both as reducing and capping agent (citrate) & provides stability to the as-synthesized Ag NPs. Briefly, the necessary volumes of freshly prepared aqueous solutions of TSC and $NaBH_4$ (Table 2.1) were mixed with vigorous stirring and heated to 60°C for 30 minutes in dark conditions to make a homogenous solution. After 30 min., the required amount of $AgNO_3$ (Table 2.1) solution was added dropwise to the mixture, and the temperature was raised to 90°C. Then, the pH of reaction mixture was adjusted to 10.5 using 0.1 M NaOH and the reaction mixture was kept at 90°C for another 20 min. The synthesized Ag NPs solution was cooled down to room temperature. The unreacted components (if any) were removed by dialysing the Ag NPs solution using a 12-kDa cut-off membrane overnight with four changes of Milli-Q water.

Table 2.1: Concentrations of various reagents for the synthesis of Ag NPs with varied sizes.

S. No.	Size of Ag NPs (nm)	$NaBH_4$ (mM)	TSC (mM)	$AgNO_3$ (mM)
1.	5	2.00	4.28	1.00
2.	10	2.00	2.00	1.17
3.	20	1.00	3.55	1.00
4.	50	0.50	2.00	1.22

For the variation in surface capping agent over Ag NPs, various capping agents were used viz. citrate (chemical agent), fucose (sugar), lysozyme (commercial protein) and biological protein (fungal proteins). Citrate capped Ag NPs (C-Ag NPs) were synthesized, as per the procedure discussed above. Coating of fucose was applied on the as-synthesized C-Ag NPs following the method described in our research article (Bhargava et al., 2018). Coating of fucose on C-Ag NPs is a two-step method, where, in the first step 3-marcaptopropionic acid (MPA) was coated on C-Ag NPs followed by functionalization with L-fucose (Kalaivani et al., 2012; Long et al., 2017). The coating of MPA on NPs is a ligand- exchange reaction where 1 mL of 20 mM MPA was added to 24 mL of C-Ag NPs with continuous stirring at room temperature (RT). The solution was stirred overnight under dark, and particles were separated by centrifugation (20,000 rpm; 30 min; RT). The obtained pellet of MPA conjugated NPs was washed multiple times with MilliQ water and re-suspended in 25 mL water. In the second step, 0.01 M of the aqueous solution of L-fucose was added dropwise to freshly prepared MPA-NPs conjugate in the ratio of 1:4.16 (v/v) with continuous stirring and the mixture was incubated overnight at RT in dark conditions. Later, the unreacted fucose was removed by centrifugation (20,000 rpm; 30 min; RT) and the fucose coated Ag NPs (F-Ag NPs) were purified by multiple washing with Milli-Q water.

Lysozyme coated Ag NPs (L-Ag NPs) were synthesized using the protocol reported by Ashraf et al. (2014). In this protocol, lysozyme functions as both reducing as well as a stabilizing agent. Typically, 2 mg of lysozyme was added to 20 ml aqueous solution of 1 mM $AgNO_3$ under vigorous stirring conditions at 120°C for 20 min. It was followed by the addition of 1 ml of 1M NaOH aqueous solution and the reaction mixture was incubated for 1 h at the same temperature. Synthesis of L-Ag NPs was confirmed by the development of light to dark-red colour as the reaction proceed.

In order to check the stability of all the synthesized Ag NPs, UV visible spectroscopy measurements were recorded after 2 months of storage at room temperature.

2.2.3 Characterization of Ag NPs

Visual characterization: Experimental flasks were visually monitored to find out the changes in the colour of the reaction mixture (colourless) after exposure to silver nitrate solutions.

UV-visible characterization: Chemical reduction of silver ions in terms of Ag NPs synthesis was examined after the completion of reaction by recording the absorption spectrum on V-630 UV-visible spectrophotometer (Jasco Corporation, Tokyo, Japan)

TEM, High-resolution TEM (HR-TEM) and selected area electron diffraction (SAED) analysis: Samples for TEM analysis were prepared by drop-coating the as-synthesized NPs samples on carbon-coated copper grids followed by vacuum drying. TEM measurements were carried out on a Hitachi H-7650 TEM instrument (Hitachi High-Technologies Corporation, Japan) at an acceleration voltage of 100 kV. HR-TEM and SAED pattern determinations were carried out using JEOL-2100 TEM instrument (JEOL, Japan) operated at an accelerating voltage of 200kV.

EDS analysis: Elemental analysis of freeze dried nanoparticle samples were carried out using a Quantax EDS attachment (Bruker AXS Ltd., Coventry, UK) equipped with scanning electron microscope (SEM). For this, samples were prepared by drop coating the Ag NPs solution on glass slide followed by overnight vacuum drying.

XRD pattern analysis: The X-ray diffraction pattern of drop coated film of Ag NPs was observed on a Rigaku MiniFlex II Benchtop XRD System (Rigaku Company, USA) operated at a voltage of 45 kV and current of 40 mA with Cu Kα radiation. The crystal phase was analyzed by comparing the calculated values of interplanar spacing and the corresponding intensities of diffraction peaks with the standard theoretical values of the Powder Diffraction File database (PCPDFWIN; JCPDS-ICDD 2008).

Zeta potential analysis: Charge present on the surface of as-synthesized Ag NPs was measured by Zetasizer Nanoseries compact scattering spectrometer (Malvern Instruments Ltd., USA).

FTIR spectroscopy measurements: FTIR analysis of the as-synthesized Ag NPs was carried out on Shimadzu IR Prestige-21 FTIR spectrometer (Shimadzu, Nakagyo-ku, Japan) with a diffuse reflectance mode (DRS-8000) attachment (Shimadzu Corporation, Nakagyo-ku, Japan). All measurements were carried out in the range of wavenumbers 400–4,000 cm^{-1} at a resolution of 4 cm^{-1}.

2.2.4 Results and discussions

(A) Variation in size

For the controlled synthesis of Ag NPs with varied sizes, the co-reduction approach was followed using two different reducing agents ($NaBH_4$ and TSC) with two step thermal reaction (Agnihotri et al., 2014). Initially, $NaBH_4$ reduces the silver cations and fabricates their nucleation at 60°C. The remaining silver cations and silver nuclei formed at the primary stage were further processed under the reduction potential of TSC at 90°C to form the fully-grown Ag NPs. Although $NaBH_4$ and TSC were added together at the start of the process, but at lower temperature, TSC supports the reduction process and prevent the formation of Ag NPs cluster, which ultimately controls the reaction. The different ratio of $NaBH_4$ and TSC used in the reaction process resulted in synthesis of Ag NPs with varied size range (5, 10, 20, and 50 nm). The size of Ag NPs can also be affected by variation in the pH. Therefore, an optimum pH of 10.5 was maintained until the completion of all the reactions.

There are many reports which demonstrated the better antimicrobial activity of the smaller NPs (Ma et al., 2011). Considering this fact in mind, we synthesized Ag NPs of small size range $\leq$ 50 nm (viz. 5, 10, 20, and 50 nm) (Table 2.1). The high surface area to volume ratio of small sized Ag NPs facilitates dissolution of more silver ions as compared to large sized Ag NPs, leading to higher antibacterial activity (Pareek et al., 2018).

All the synthesized Ag NPs were characterized by various standard techniques. As the synthesis of Ag NPs occurred, the colour of reaction mixture gradually turned from colourless to dark brown. The intensity of colour depended on the size of NPs (Insets of Figure 2.1). This transformation in the colour of reaction mixture was due to the surface plasmon resonance (SPR) at the surface of Ag NPs (Singh et al., 2018), which was further confirmed by the UV-visible spectroscopy analysis of reaction mixture after the completion of reaction. The UV-visible absorption maxima of Ag NPs was found to vary with their size due to the SPR effect. UV-visible absorption maxima was recorded to be 395, 394, 406, and 411 nm for the average particle size of 5, 10, 20, and 50 nm, respectively (Figure 2.1). The stability of the synthesized Ag NPs solutions stored at room temperature in dark condition was confirmed by the presence of SPR peak of same intensity after a period of 2 months.

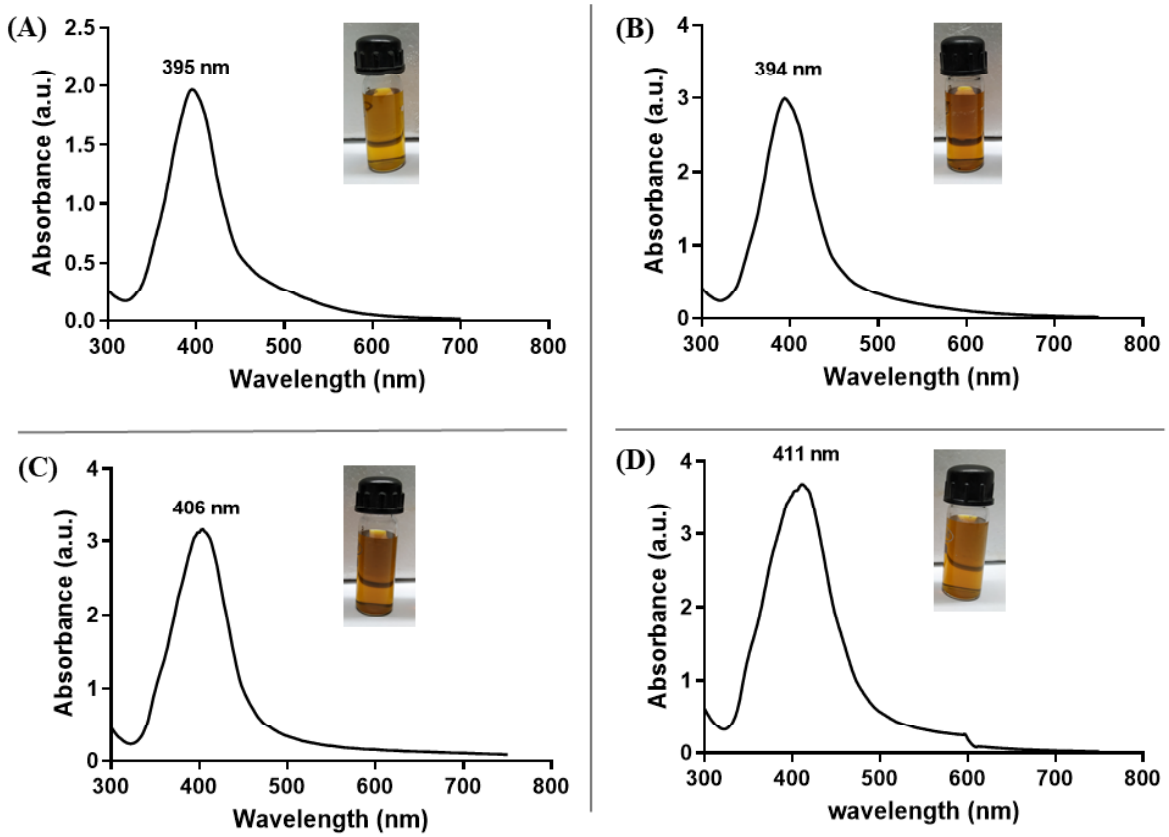

Figure 2.1: UV-visible spectra of chemically synthesized Ag NPs of varied sizes (A) 5 nm, (B) 10 nm, (C) 20 nm and (D) 50 nm. Inset of these figures shows the colour of the reaction mixture after the completion of reaction.

TEM analysis was performed to check the morphology and size of all the synthesized Ag NPs. The obtained TEM micrograph revealed mono-dispersed and quasi-spherical nature of all the synthesized Ag NPs except 50 nm particles (Figure 2.2 A). The particle size histogram was prepared by counting ~ 200 NPs using multiple TEM micrographs separately for each size (Figure 2.2 B). The details on particle size range determination using TEM analysis has been provided in Table 2.2. Although slight variations were observed in the obtained average particle size as compared to the report of Agnihotri et al. (2014), for convenience, we have designated 5, 10, 20 and 50 nm sizes in further chapters.

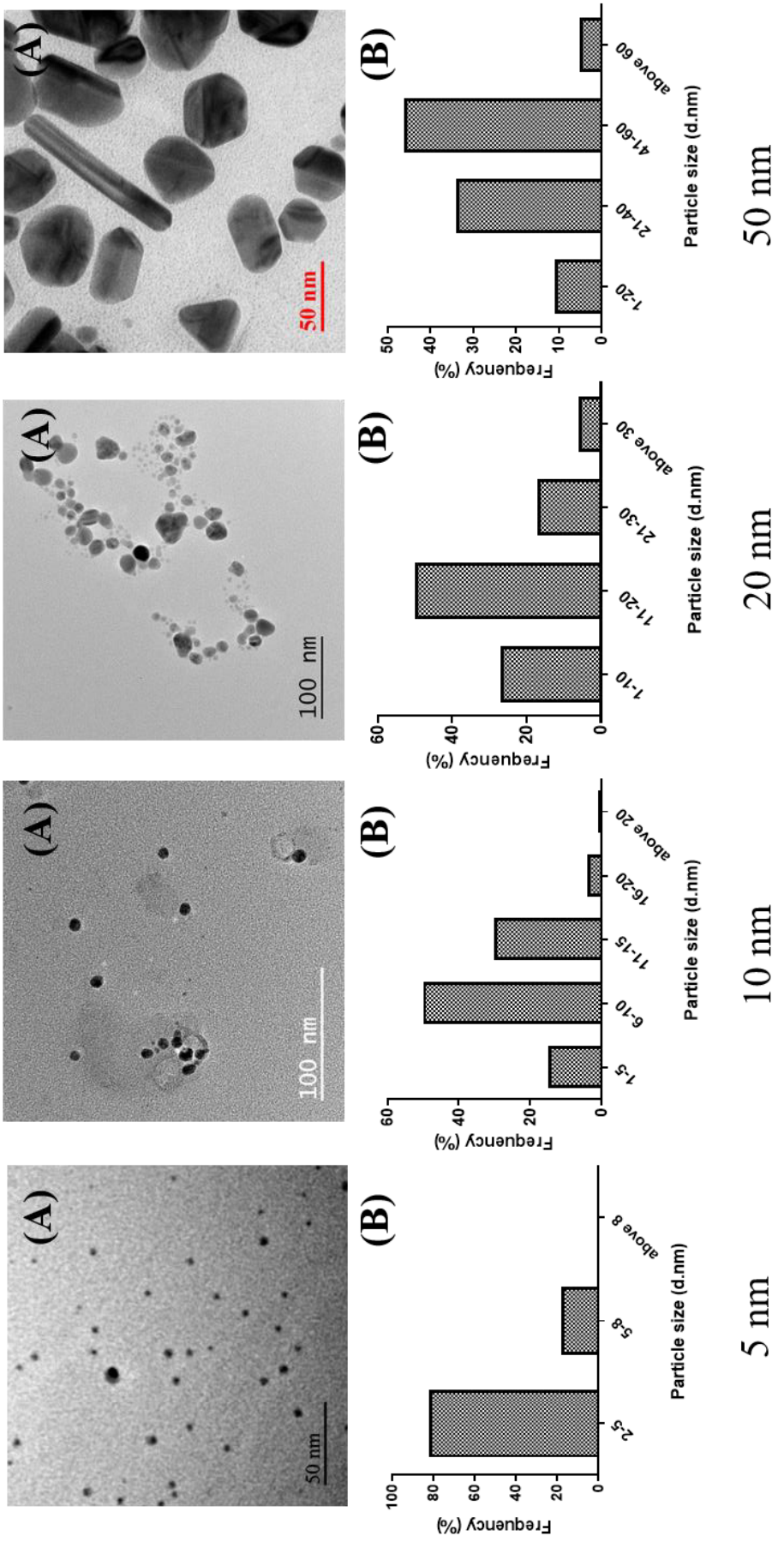

Figure 2.2 (A) TEM micrographs and (B) particle size histograms of chemically synthesized Ag NPs of varied sizes (5, 10, 20 and 50 nm)

Table 2.2: Particle size analysis of chemically synthesized Ag NPs of varied sizes determined using TEM analysis.

S. No.	Expected size of Ag NPs (nm) as per Agnihotri et al. (2014)	Observed average particle size (nm) of synthesized Ag NPs
1.	5	6.4 ± 1.6
2.	10	9.5 ± 3.5
3.	20	17.1 ± 3.9
4.	50	46.0 ± 5.7

Owing to the smaller de Broglie wavelengths of electrons, the structural aspects of individual NP's atomic organization were observed by HR-TEM analysis, which confirmed round edges and no crystallinity defect in all the synthesized Ag NPs (Figure 2.3A). The lattice fringes observed in HR-TEM micrograph further represented the crystalline nature of synthesized Ag NPs (Knowles, 2001). The SAED pattern of one of the representative Ag NPs of respective size (Figure 2.3 B) authenticated the crystal plane (111) of synthesized Ag NPs depicting face centered cubic (fcc) lattice structure of crystalline silver (Mishra et al., 2007; Jiang et al., 2011; Tsai et al., 2013). These results are in alignment with previous reports (Jain et al., 2011; Agnihotri et al., 2014).

EDS analysis of freeze-dried Ag NPs was performed to determine their elemental composition (Figure 2.4). Presence of optical absorption band at 3.0 and 0.25 keV validated the presence of Ag metal. In addition, peaks for silicon, sodium, oxygen, and carbon were also observed at 1.76, 1.0, 0.5, and 0.27 keV, respectively, due to the coating of citrate capped NPs on glass slide during sample preparation (Magudapathy et al., 2001; Ji et al., 2010; Zhang et al., 2011; Ahmad et al., 2012; Tsai et al., 2013).

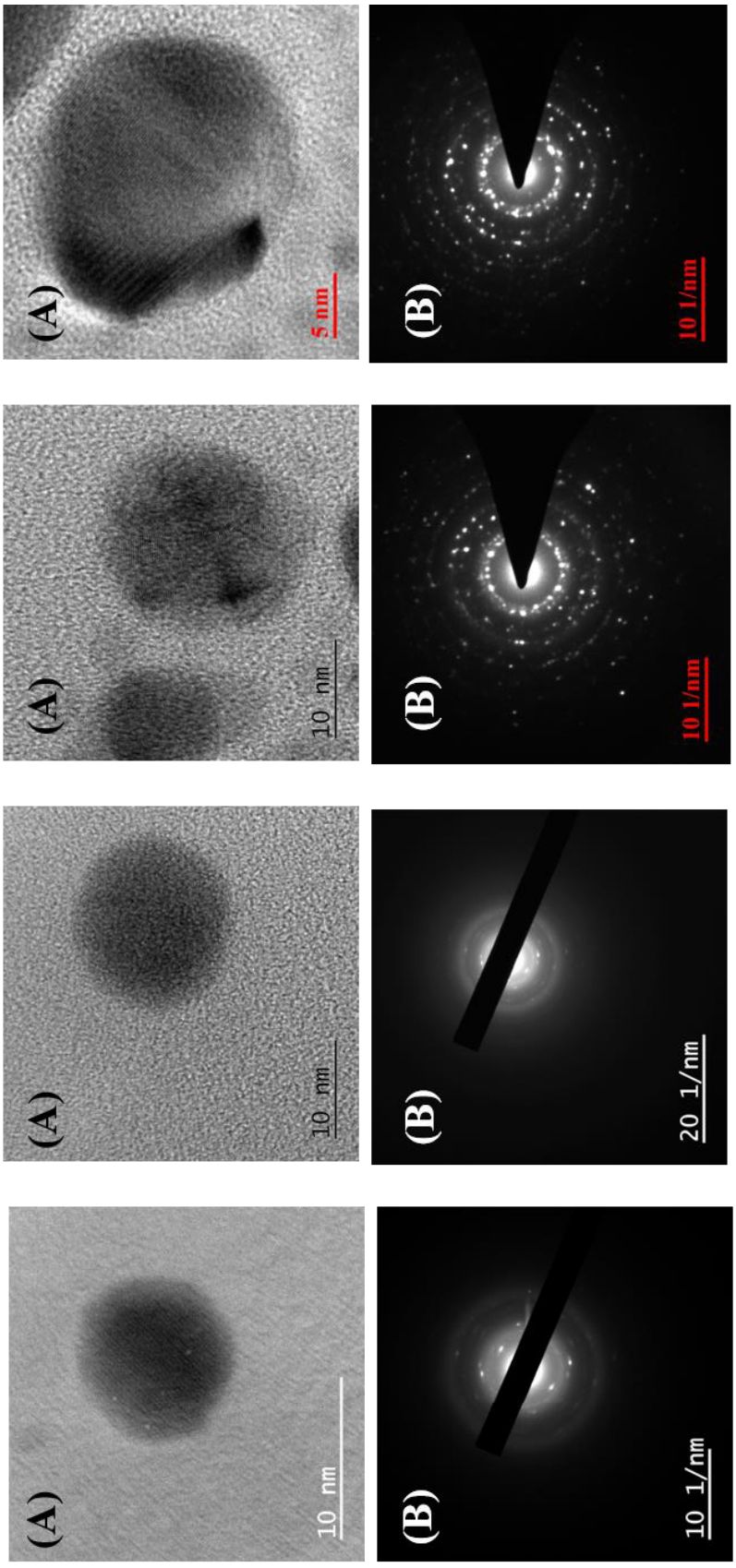

Figure 2.3: Representative image of (A) HR-TEM and (B) SAED pattern of respective Ag NPs

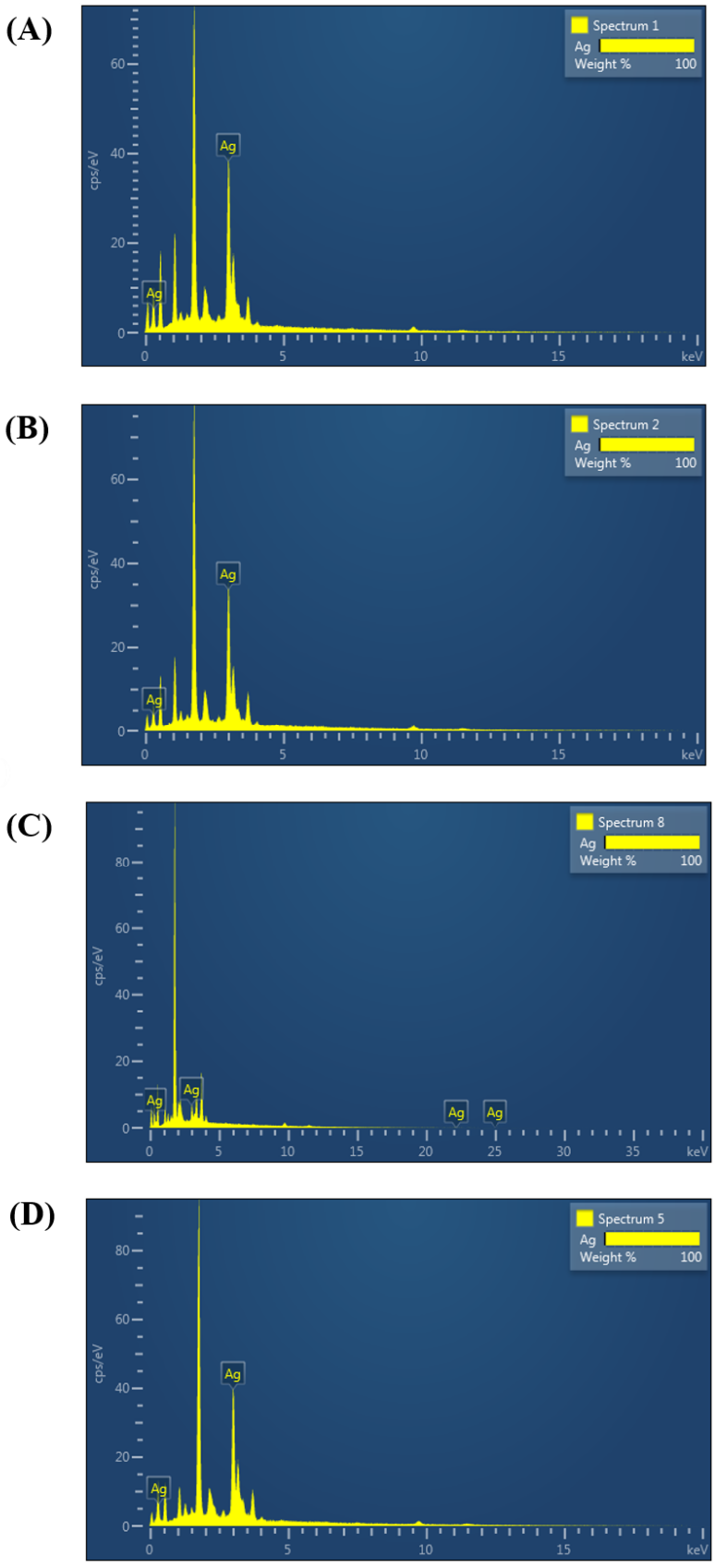

Figure 2.4: EDS spectrum showing the presence of elemental silver in chemically synthesized Ag NPs of varied sizes (A) 5 nm, (B) 10 nm, (C) 20 nm, and (D) 50 nm.

Diffraction pattern of drop coated Ag NPs was recorded by XRD measurement (Figure 2.5). The observed Bragg's reflections exhibited fcc crystalline structure in all the synthesized Ag NPs with well-defined peaks at the 2θ value of 38.25°, 46.26°, 64.70° and 77.66°, which correspond to (111), (200), (220) and (300) planes of silver, respectively, as per file no. 04-0783 of Joint Committee on Powder Diffraction Standards (*JCPDS*) of International Centre for Diffraction Data (ICDD) Database. One of the representative image of XRD analysis among all chemically synthesized Ag NPs is depicted in Figure 2.5 (Khanna et al., 2005; Kim et al., 2006; Mishra et al., 2007).

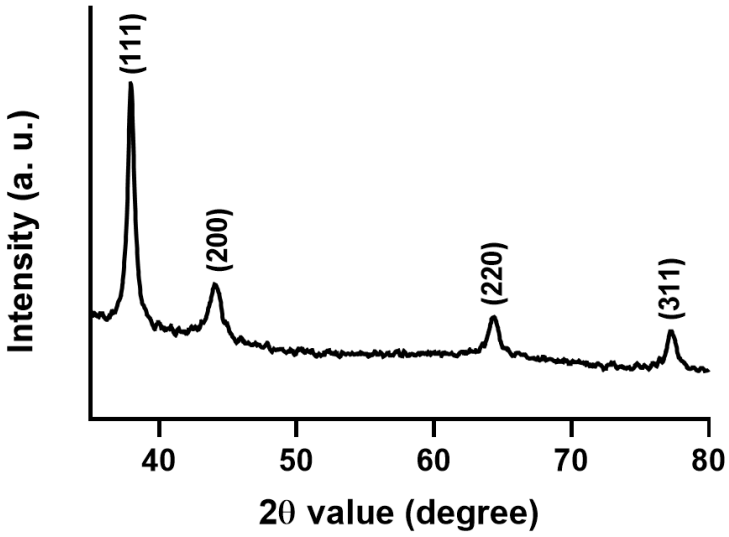

Figure 2.5: Representative XRD image of chemically synthesized Ag NPs.

The obtained zeta potential (ζ) values for 5, 10, 20, and 50 nm were found to be -37.0 ± 0.7, -18.8 ± 1.9, -30.2 ± 1.9, and -33.8 ± 1.2 mV, respectively. The negative zeta potential values were due to the presence of citrate as surface capping agent (Salvioni et al., 2017). Presence of carboxylic group in citrate provide negative charge to the Ag NPs and allowed NPs to disperse without aggregation (Park and Lee, 2013; Salvioni et al., 2017).

FTIR analysis further confirmed the presence of citrate as capping material for all the synthesized Ag NPs. FTIR analysis of freeze-dried samples showed characteristic infrared bands at 1425 and 1430 cm^{-1}, which referred to the bending vibrations in CH_2 and CH_3 groups, respectively. Presence of bands at 1630 and 3401 cm^{-1} correspond to the C=C and OH stretching vibrations, respectively (Figure 2.6; Agnihotri et al., 2014).

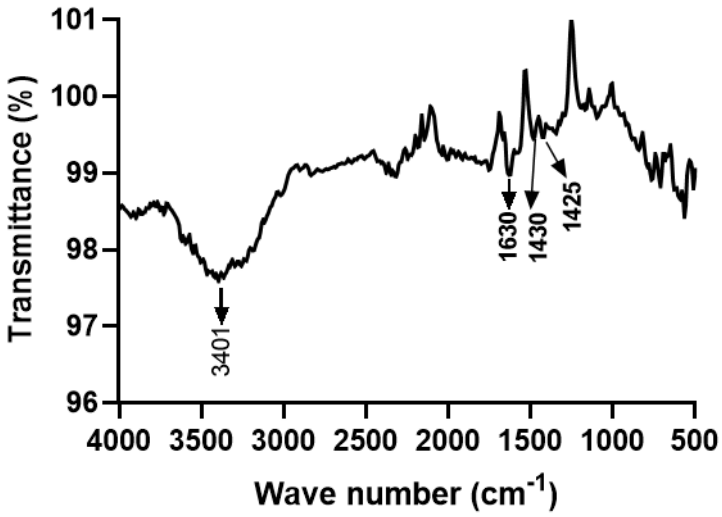

Figure 2.6: Representative FTIR image of chemically synthesized Ag NPs.

(B) Variation in surface capping

In order to check the effect of various surface capping agents on the antibacterial potential of Ag NPs, initially the chemically synthesized Ag NPs of all sizes (5, 10, 20 and 50 nm) were screened for their antibacterial activity by minimum inhibitory concentration (MIC) assay (discussed in chapter 3). The obtained results revealed that the antibacterial potential of Ag NPs was inversely proportional to the size. These results were consistent with the earlier report of Martinez-Castanon et al. (2008). Hence, Ag NPs of smaller size range (5-20 nm) were selected to study the effect of various surface coating agents towards their antibacterial potential.

Based on the literature survey, citrate, L-fucose, lysozyme and fungal proteins as chemical agent, sugar, commercial protein, and biological protein, respectively were selected for the surface coating of Ag NPs. Citrate as a chemical agent was selected among many others because of its high chemical stability and solubility potential in polar solutions, which can make Ag NPs chemically more stable and soluble (Thio et al., 2011, Gutierrez et al., 2015). Citrate capped Ag NPs (C-Ag NPs) of 5 nm size were synthesized by the co-reduction method, where citrate function as both reducing and surface capping/stabilizing agent (Agnihotri et al., 2014). The absorption spectrum of C-Ag NPs showed presence of SPR peak at 395 nm (Figure 2.7 A).

Fucose is a six-carbon, L-formed sugar found profusely in mammalian gut's epithelial layer. It is the rarest form of sugar available in L-form. In the mammalian gut, fucose is used by the various gut symbiont bacterial species, which possess the enzyme (α-fucosidase) to hydrolyze fucose (Fabich et al., 2008; Kamada et al., 2012; Pickard and Chervonsky, 2015). Keeping this fact in mind, we hypothesized that capping of fucose on Ag NPs could attract bacteria to utilize fucose as energy source, which will enhance the probability of Ag NPs interactions with bacteria. For coating of fucose, the as-synthesized C-Ag NPs (5 nm) were used. L-fucose (sugar) was functionalized on C-Ag NPs by initial capping of MPA, which mediates subsequent capping of L-fucose by ligand exchange chemistry (Kennedy et al., 2014). Use of MPA for the binding of L-fucose leads to slight accumulation of NPs, which eventually caused a decrease in the intensity of SPR peak and red shift in the absorption maxima (420 nm) (Figure 2.7 B).

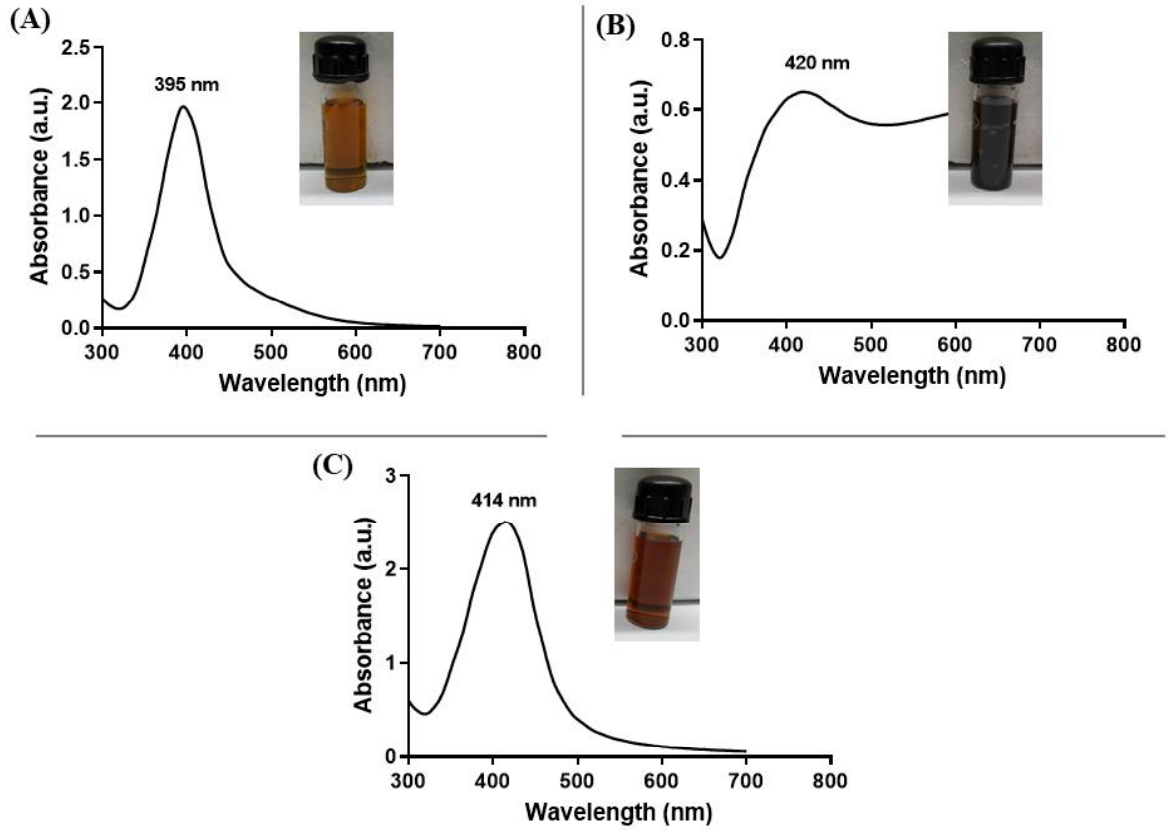

Figure 2.7: UV visible spectra of Ag NPs with variation in their surface capping viz. (A) citrate, (B) fucose, and (C) lysozyme.

In nature, lysozyme exists in tears, sweat, saliva, and other body fluids of higher organisms. It prevents the attack of bacterial infections by acting directly on the peptidoglycan layer of bacteria. It is a glycoside hydrolase enzyme which mainly acts on β-1,4 linkages between the N-acetylmuramic acid and N-acetyl-D-glucosamine units of peptidoglycan layer (Eby et al., 2009). As discussed in the previous chapter, gram-negative bacteria have a very thin peptidoglycan layer covered by the lipopolysaccharide outer membrane, which prevents the action of lysozyme on this category of bacteria. Coating of denatured form of lysozyme (positively charged) on Ag NPs can increase their interaction with the negatively charged bacterial outer membrane. Considering this, lysozyme was selected as a commercial protein in order to cap the surface of Ag NPs. Lysozyme coated Ag NPs (L-Ag NPs) were synthesized by the co-reduction method in which lysozyme function as both reducing and stabilizing agent (Ashraf et al., 2014). This co-reduction was achieved by the heat reflux action at 120°C, which leads to the coating of a denatured form of lysozyme on the Ag NPs. Denaturation or perturbation of native protein structure at this high temperature leads to inactivation of enzyme activity (Ibrahim et al., 1996; Eby et al., 2009). This suggests that denatured lysozyme molecule will act only as the capping material and cannot show enzymatic action on the bacterial cell. Synthesis of L-Ag NPs was visualized by the development of light to dark-red colour of solution as the reaction proceeds and was further confirmed by the UV-visible spectroscopy analysis of reaction mixture, which showed an absorption maxima peak at 414 nm (Figure 2.7 C). The stability of the C-Ag NPs, F-Ag NPs, and L-Ag NPs solutions stored at room temperature in dark conditions for 2 months after completion of reactions were confirmed by the UV-visible spectroscopy measurements. It was observed that the nanoparticle solutions were stable at room temperature, with no evidence of particle aggregation as determined by UV-visible spectroscopy measurements.

The morphology and size of C-Ag NPs, F-Ag NPs, and L-Ag NPs was measured by TEM analysis. Representative TEM micrographs of C-Ag NPs, F-Ag NPs and L-Ag NPs along with their respective particle size histogram extracted from the TEM micrograph are shown in Figure 2.8. The obtained TEM micrograph revealed mono-dispersed and quasi-spherical nature of all the synthesized Ag NPs. The effect of varying surface coating agents on the particle size of Ag NPs has been represented in Table 2.3.

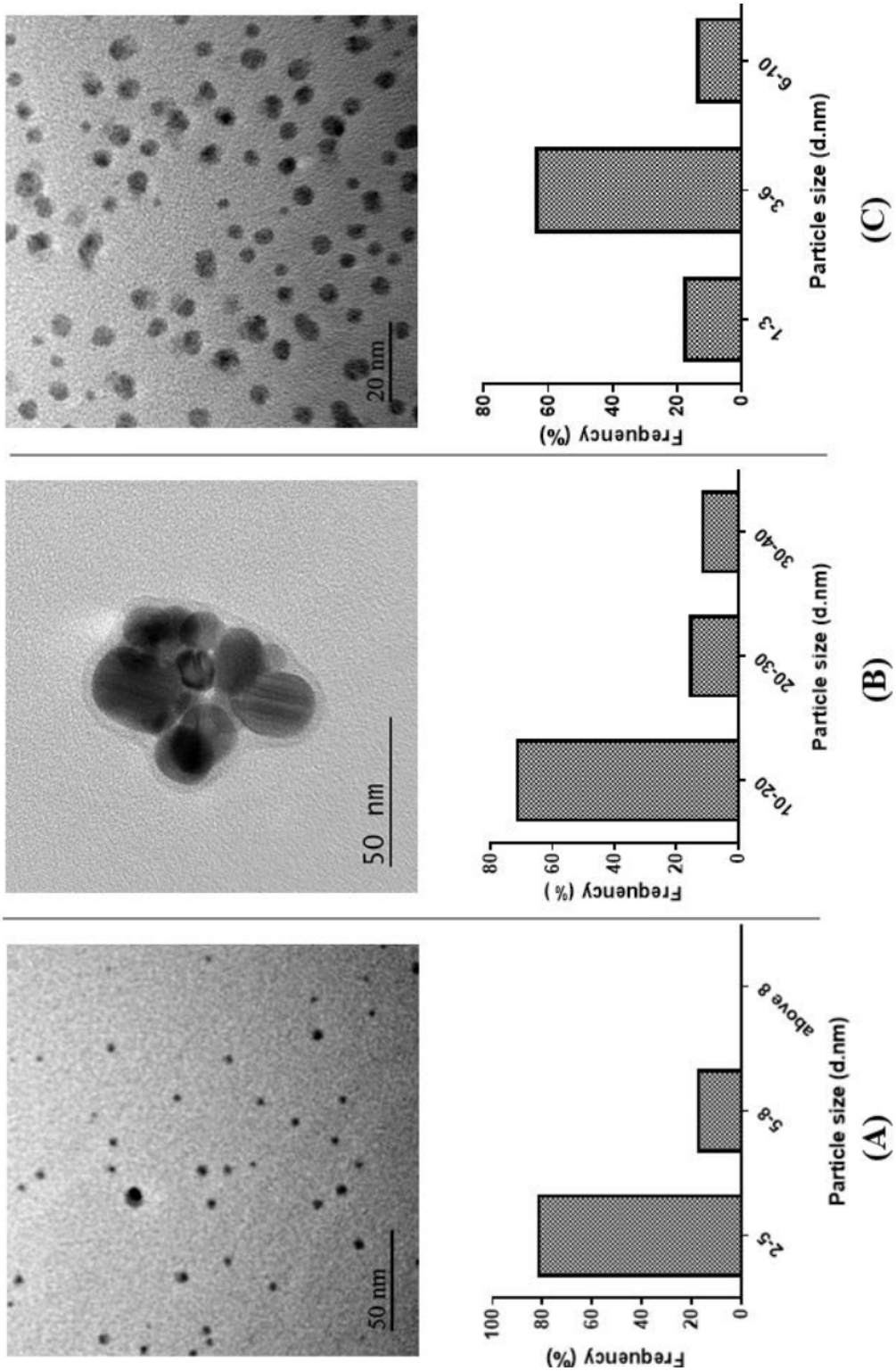

Figure 2.8: TEM micrograph and particle size histogram of Ag NPs with variation in their surface capping by (A) citrate, (B) fucose and (C) lysozyme

Table 2.3: Particle size of Ag NPs with variation in their surface capping determined using TEM analysis.

S. No.	Surface coating agent	Size range of particles (nm)	Average particle size (nm)
1.	Citrate	2 - 8	6.4 ± 1.6
2.	Fucose	10 - 40	22.5 ± 1.8
3.	Lysozyme	1-10	5.2 ± 1.2

To confirm the elemental composition, EDS spectrum of Ag NPs with varied capping agents was recorded (Figure 2.9). Presence of optical absorption band at 3.0 and 0.25 keV validated the presence of Ag metal in all the NPs types (Ji et al., 2010; Zhang et al., 2011; Tsai et al., 2013). As the samples for EDS analysis were prepared by drop coating Ag NPs on glass slide, additional peaks at 1.76, 1.0, 0.5, and 0.27 keV corresponding to silicon, sodium, oxygen, and carbon, respectively were also observed.

Diffraction pattern of drop coated Ag NPs with varying capping agents was recorded by XRD measurement (Figure 2.10). Well-defined peaks at the 2θ value of 38.25°, 46.26°, 64.70° and 77.66° were observed for C-Ag NPs, F-Ag NPs and L-Ag NPs, which corresponded to (111), (200), (220) and (311) planes of silver, respectively as per JCPDS file 04-0783. Diffraction pattern of drop coated Ag NPs with varying capping agents was recorded by XRD measurement (Figure 2.10). Well-defined peaks at the 2θ value of 38.25°, 46.26°, 64.70° and 77.66° were observed in all NPs types (C-Ag NPs, F-Ag NPs and L-Ag NPs), which corresponded to (111), (200), (220) and (311) planes of silver, respectively as per JCPDS file no. 04-0783. In the present study, the variations observed in the peak intensity were due to the presence of varying surface capping agents. Ajitha et al. (2016) also reported variations in the peak intensity in the XRD spectra of Ag NPs coated with polyethylene glycol, ethylene diamine tetraacetic acid, polyvinyl pyrrolidone, and polyvinyl alcohol.

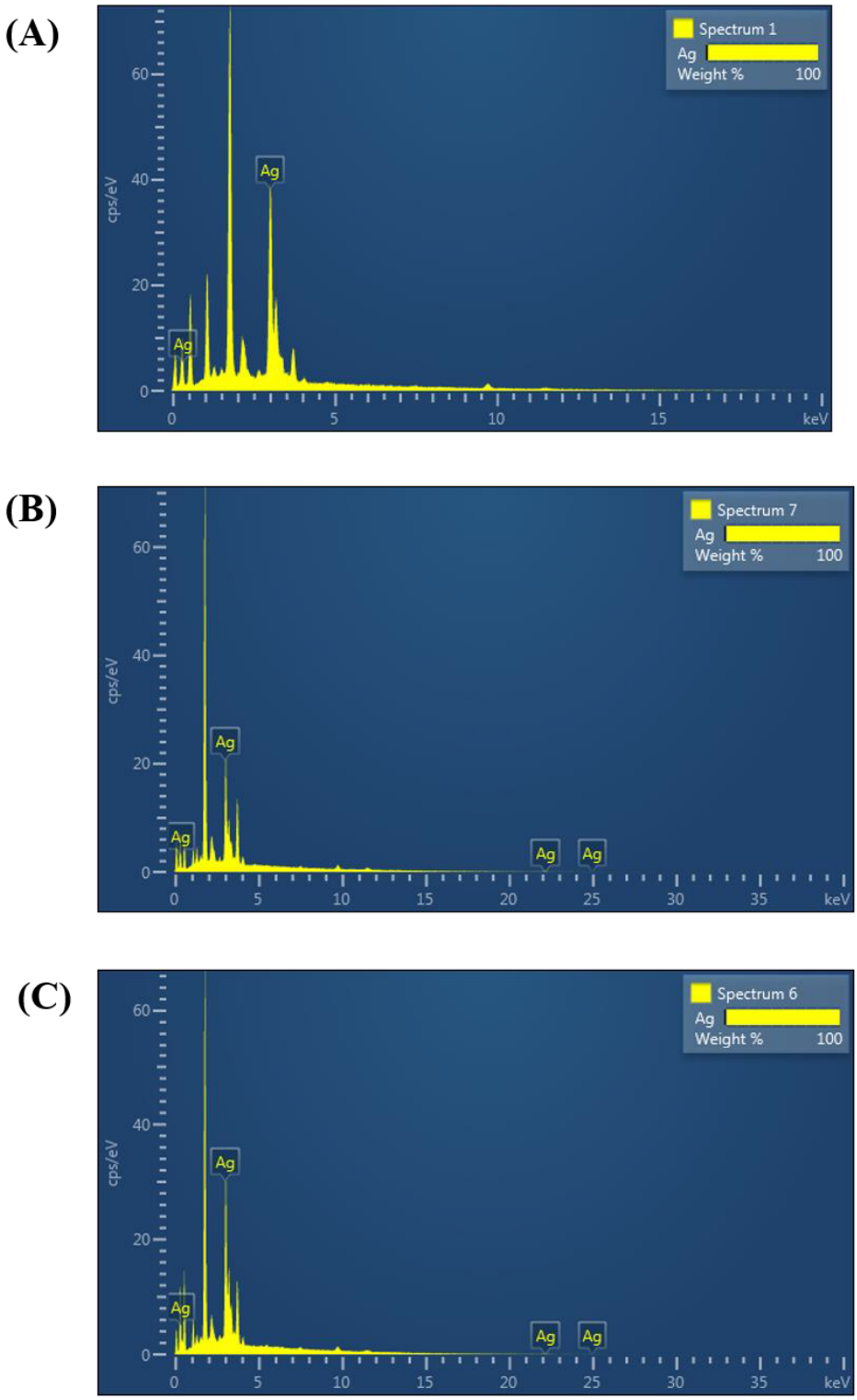

Figure 2.9: EDS spectrum showing the presence of elemental silver for Ag NPs coated with (A) citrate, (B) fucose, and (C) lysozyme.

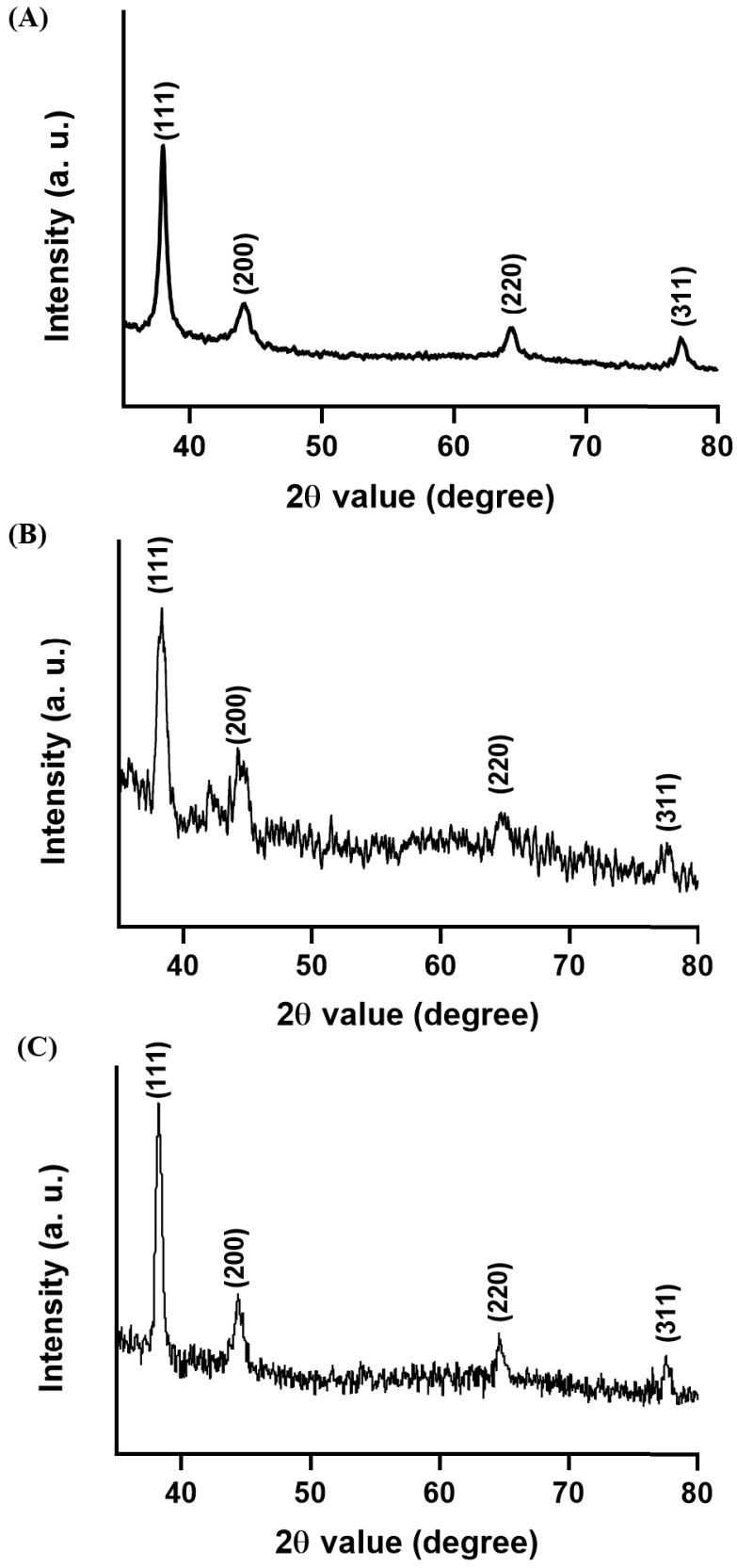

Figure 2.10: XRD pattern analysis of Ag NPs with varying surface capping (A) citrate, (B) fucose and (C) lysozyme.

Charge on the surface of Ag NPs with varied surface capping was measured using zeta potential analysis. All Ag NPs types i.e. C-Ag NPs, F-Ag NPs and L-Ag NPs were found to have negatively charged surface with zeta potential values of -37.0 ± 0.6, -17.5 ± 0.9, and -33.6 ± 1.3 mV, respectively. In case of C-Ag NPs, presence of carboxylic moiety in citrate provided negative charge (Salvioni et al., 2017). The negative zeta potential values of F-Ag NPs were due to the presence of carbonic, sulfonic, and hydroxyl groups on the surface of NPs (Altankov et al., 2003; Bhargava et al., 2018). Although, the intact lysozyme is a positively charged protein, due to the denaturation of lysozyme at very high temperature (120°C) during the synthesis of L-Ag NPs, it provided a negative charge to NPs (Ibrahim et al., 1996).

FTIR measurements were performed to check the surface capping of as-synthesized Ag NPs. FTIR analysis of C-Ag NPs showed characteristic infrared bands at 1425 and 1430 cm^{-1}, which referred to the bending vibrations in CH_2 and CH_3 groups, respectively. In addition, bands at 1630 and 3401 cm^{-1}, correspond to stretching vibration of C=C and O-H, respectively (Figure 2.11A). The presence of carboxyl groups of citrate on the surface of Ag NPs have been reported to enhance the capping stability (Long et al., 2017). Surface capping of Ag NPs by L-fucose can be confirmed by the presence of various chemical bonds present in the chemical structure of L-fucose viz. O-H, C-O, C=C etc. (NCBI, PubChem database). In the synthesized F-Ag NPs, presence of characteristic peaks at 3303, 2078, 1670, and 1262 cm^{-1} showed stretching vibration of O-H, -C=-C, non-conjugated C=C, and C-O bands respectively, which confirmed the presence of fucose on NPs (Figure 2.11B). Presence of lysozyme on Ag NPs was confirmed by the characteristic peaks at 3260 and 1632 cm^{-1}, which represents the stretching vibrations of N-H and amide I bond, respectively (Figure 2.11C). These chemical bonds are responsible for the formation of peptide bond in proteins. Considering the proteinaceous nature of lysozyme, these bonds appeared in FTIR spectra of L-Ag NPs (Baker et al., 2014; Ashraf et al., 2014).

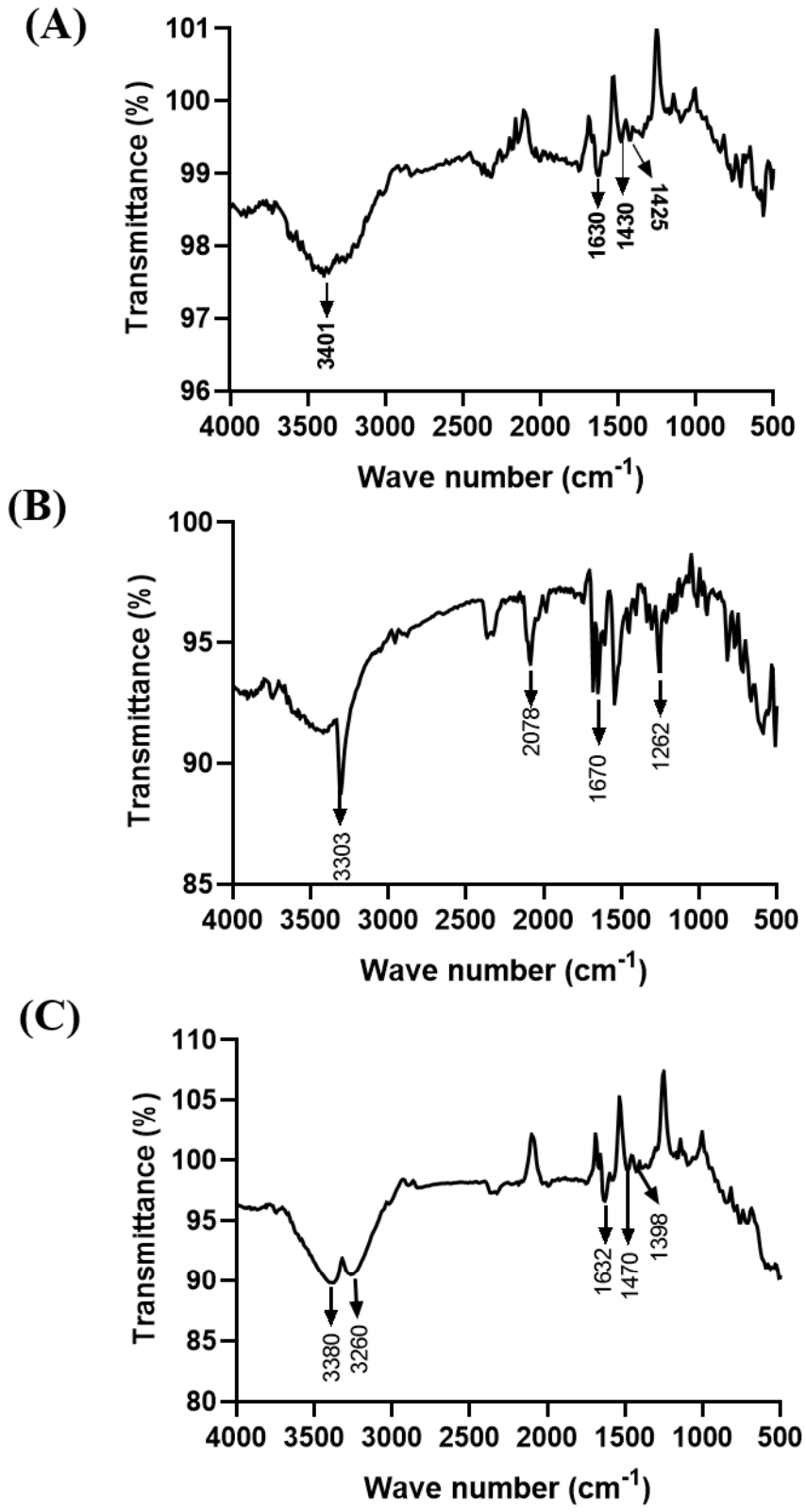

Figure 2.11: FTIR analysis of Ag NPs with varying surface capping (A) citrate, (B) fucose and (C) lysozyme.

2.3 Biological reduction method

Based on the organism type, the attempts to synthesize NPs using biological entities can be divided into two broad groups. One group comprises of prokaryotic organisms such as bacteria and the other group includes multicellular eukaryotic organisms such as algae, fungi, and plants. Due to the simplicity of the structures and metabolism, prokaryotes are the first choice for NPs synthesis. However, prokaryote mediated NPs synthesis suffers various disadvantages such as difficult handling, less versatile secretome and low synthesis efficiency due to on-cell/ intracellular NP synthesis (Pareek et al., 2017). In recent years, eukaryotic organisms especially fungi have emerged as a potential candidate for the extracellular synthesis of NPs due to their ease in handling, low maintenance cost, and easy downstream processing (Bhargava et al., 2013). In addition, being eukaryote, fungi have been reported to secrete a versatile range of extracellular metabolites in large quantity as compared to prokaryotic organisms, which allow extracellular NP synthesis (Bhargava et al., 2016). In our laboratory, we have successfully developed and demonstrated environmental friendly and cost-effective methods for the on-cell and extracellular synthesis of Ag NPs (Jain et al., 2011; Bhargava et al., 2015; Fageria et al., 2017).

In the present study, two different metal tolerant soil fungi *Penicillium shearii* AJP05 and *Penicillium janthinellum* DJP06 were selected from the available fungal isolates in our research group (Bhargava et al., 2016). Attempts were made to synthesize Ag NPs following both indigenously developed on-cell and extracellular synthesis methods (Jain et al., 2011; Bhargava et al., 2015). In case of on-cell synthesis method, fungal mycelia were directly exposed to precursor salt solution whereas, in extracellular synthesis method, the fungal cell free filtrate was exposed to precursor salt solution. However, on-cell synthesis method could not show any positive results (data not shown). For the extracellular synthesis of Ag NPs, actively growing culture of selected fungal isolates were separately inoculated in 100 ml of MGYP medium (0.3 % malt extract, 1.0 % glucose, 0.3 % yeast extract, 0.5 % peptone digest; pH 7.0) in 250 ml Erlenmeyer flasks and incubated under dark conditions at 28°C for 72 h on a rotary shaker (150 rpm). After incubation, the biomass was separated from the media by centrifugation (5000 rpm, 10 min., 4°C) followed by washing with milli-Q water to remove all traces of media. In order to collect the fungal secretome (extracellular filtrate), 20 g of fungal biomass (fresh weight) was resuspended in 100 ml of sterile milli-Q water and further incubated for 72 h under similar conditions described above. After Incubation, the fungal secretome containing extracellular metabolites was separated and collected by vacuum

filtration. For synthesizing Ag NPs, 100 ml of fungal secretome was exposed to aqueous solution of $AgNO_3$ at a final concentration of 1.0 mM. The flasks were further incubated for 72 h under similar conditions described above. Flasks containing only fungal secretome and only $AgNO_3$ aqueous solution were also incubated simultaneously as a positive and negative control, respectively. The experiments were performed in triplicates.

2.3.1 Characterization of Ag NPs

Characterization of myco-synthesized Ag NPs was performed by various standard techniques including visible monitoring, UV visible spectroscopy, XRD, FTIR, TEM, HR-TEM, SAED, and EDS analysis, as discussed earlier in section 2.2.3

2.3.2 Results and Discussions

After the addition of precursor salt, the fungal secretome gradually changed from colourless to dark brown colour (Inset of Figure 2.12 A and B). No change in the colour was observed in respective negative control flasks, which signified the involvement of fungal extracellular metabolites in the reduction of silver ions and subsequent synthesis of Ag NPs. In order to find out the active metabolites, fungal secretome fraction without proteins (obtained after protein precipitation) was exposed to precursor ions. However, it showed no evidence of Ag NPs synthesis (data not shown), which indicated that proteins may be involved in the synthesis process. The observed transformation in the colour of fungal secretome was due to the surface plasmon resonance (SPR) at the surface of synthesized Ag NPs (Singh et al., 2018). Gradual synthesis of Ag NPs was also quantitated and confirmed by UV-visible spectroscopy analysis of reaction mixture at regular time intervals. Time-dependent increase in the intensity of absorption at around 446 nm and 410 nm was observed in *Penicillium shearii* AJP05 and *Penicillium janthinellum* DJP06, respectively (Figure 2.12 A and B), which denotes the gradual synthesis of Ag NPs (Fageria et al., 2017; Saravanan et al., 2018; Tomer et al., 2019). The reaction saturation curve reflected the completion of Ag NPs synthesis reaction at 1 h and 120 h for *Penicillium shearii* AJP05 and *Penicillium janthinellum* DJP06, respectively (Figure 2.12 C and D). The obtained sigmoidal graph suggested the enzyme-catalyzed nature of synthesis reaction. No SPR peak was observed in negative control (only extracellular filtrate) which suggested that synthesis reaction was not temporal in both the fungal species. The as-synthesized Ag NPs solutions were stored at room temperature and their stability was regularly monitored up to 3 months of reaction completion. Similar intensity

of SPR peak was observed up to 4 months which confirmed that the Ag NPs solution was stable at room temperature.

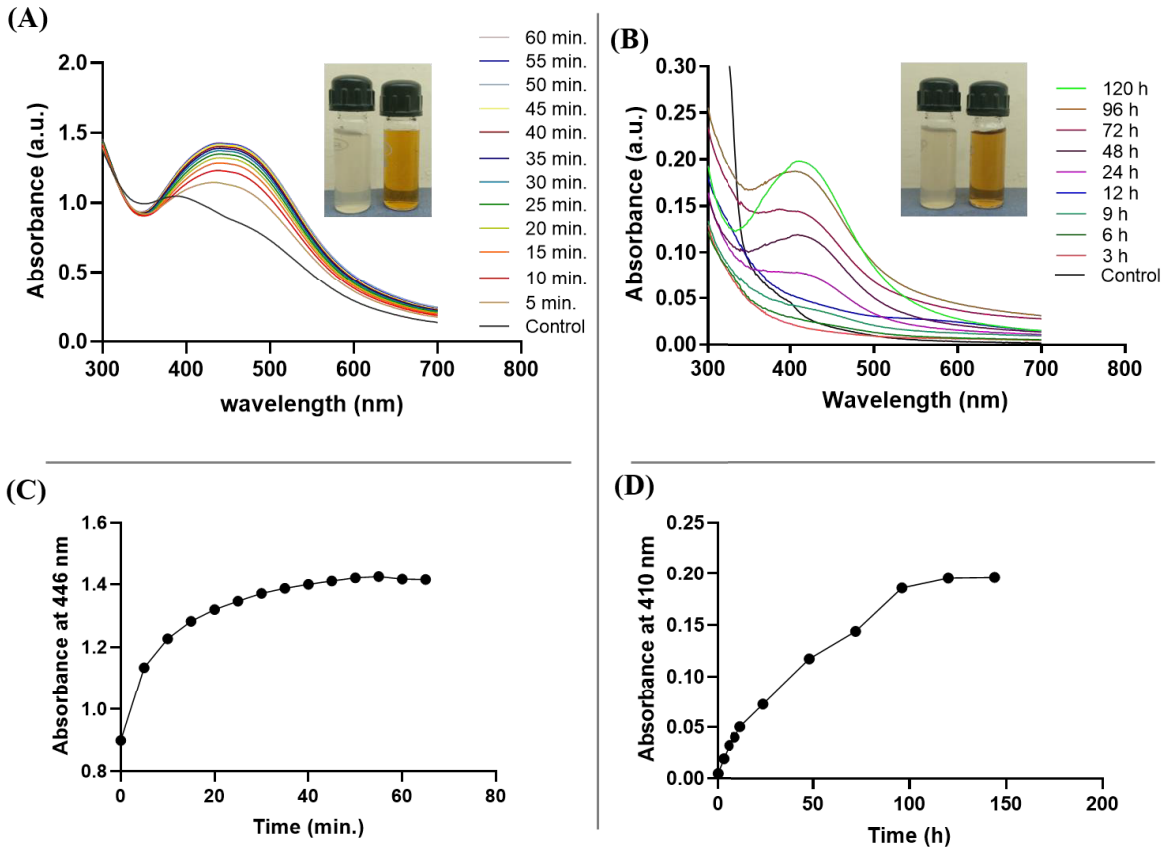

Figure 2.12: UV- visible spectra of extracellular filtrate with respect to time for (A) *Penicillium shearii* AJP05 (B) *Penicillium janthinellum* DJP06. Inset shows the synthesized Ag NPs (brown) with respect to control (colourless). Reaction saturation curve for (C) *Penicillium shearii* AJP05, and (D) *Penicillium janthinellum* DJP06.

TEM analysis was performed to check the morphology and size of as-synthesized Ag NPs. The obtained TEM micrograph revealed synthesis of mono-dispersed and quasi-spherical Ag NPs by both the test fungal species (Figure 2.13). The particle size histogram extracted from the representative TEM micrographs showed that the size of Ag NPs, ranged between the 3-20 nm with an average particle size of 8.0 ± 2.7 nm for *Penicillium shearii* AJP05. Whereas, the size of Ag NPs synthesized by *Penicillium janthinellum* DJP06 ranged between 1-30 nm with an average particle size of 12 ± 2.7 nm (Figure 2.13).

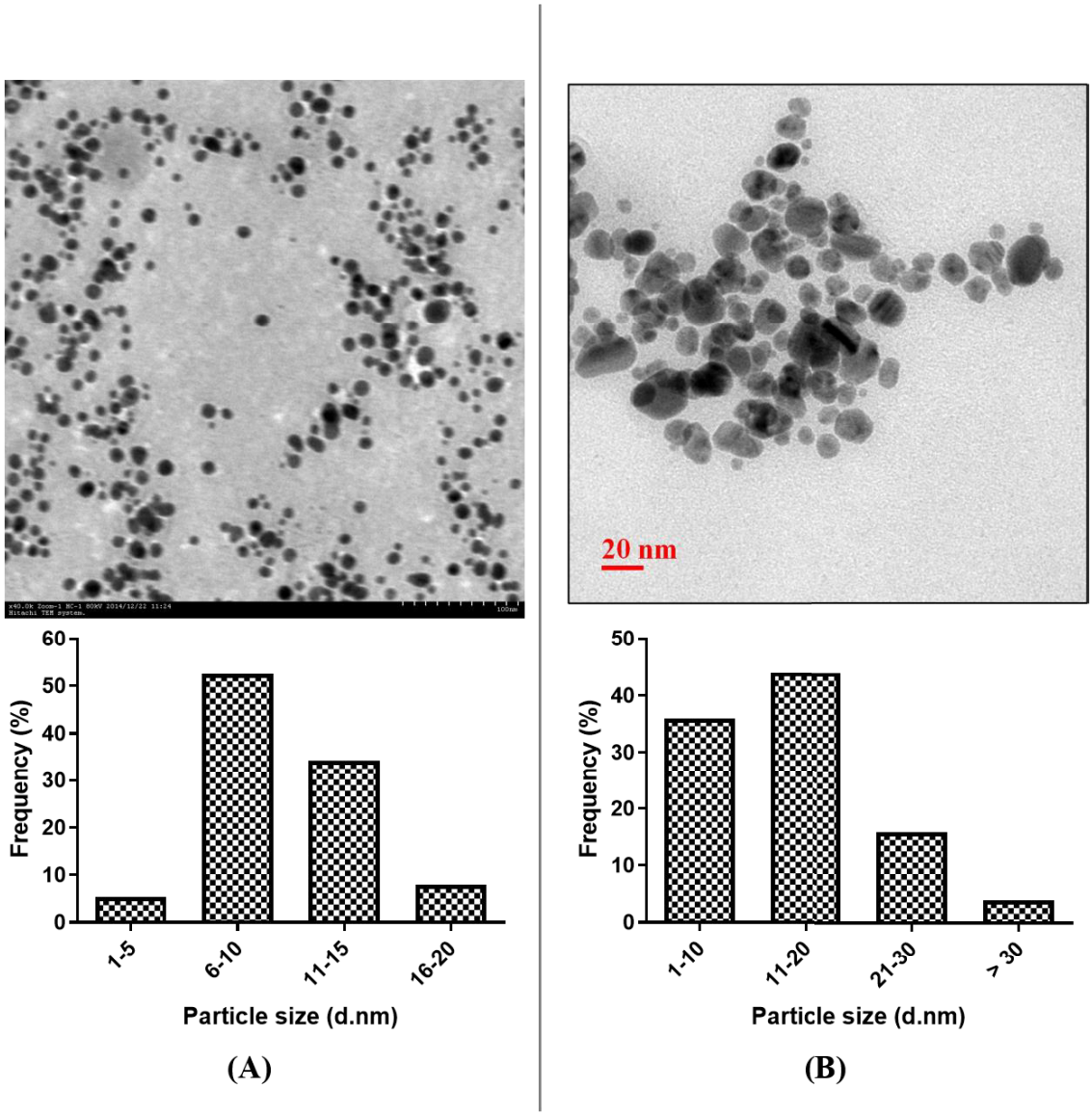

Figure 2.13: TEM micrographs and particle size histograms of Ag NPs synthesized by (A) *Penicillium shearii* AJP05, and (B) *Penicillium janthinellum* DJP06.

EDS spectrum of freeze-dried Ag NPs synthesized by both test fungus species was recorded to measure their elemental composition (Figure 2.14). Presence of silver metal with distinct peak at 3.0 keV was observed in Ag NPs, which was in alignment with the previous reports (Jain et al., 2011; Tomer et al., 2019). In case of *Penicillium shearii* AJP05, additional peaks at 1.76, 1.0, 0.5, and 0.27 keV were observed which correspond to silicon, sodium, oxygen, and carbon respectively, which was due to the coating of NPs on glass slide during sample preparation (Figure 2.14 A). In case of *Penicillium janthinellum* DJP06, as the NPs were drop coated on carbon coated copper grid, peaks for carbon (0.27keV) and copper (0.93 and 8.04 keV) were also observed (Figure 2.14 B).

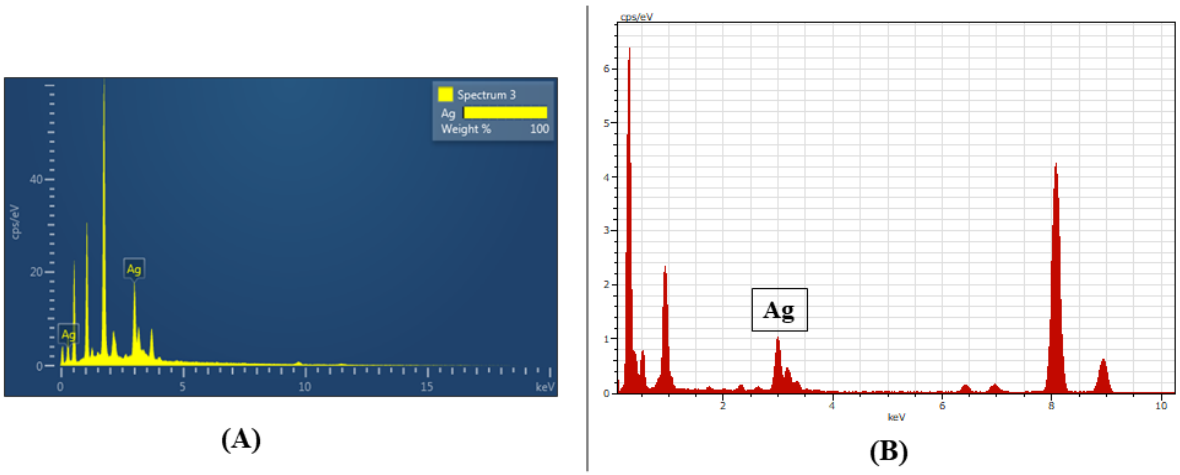

Figure 2.14: EDS spectra representing presence of silver in Ag NPs synthesized by (A) *Penicillium shearii* AJP05 and (B) *Penicillium janthinellum* DJP06.

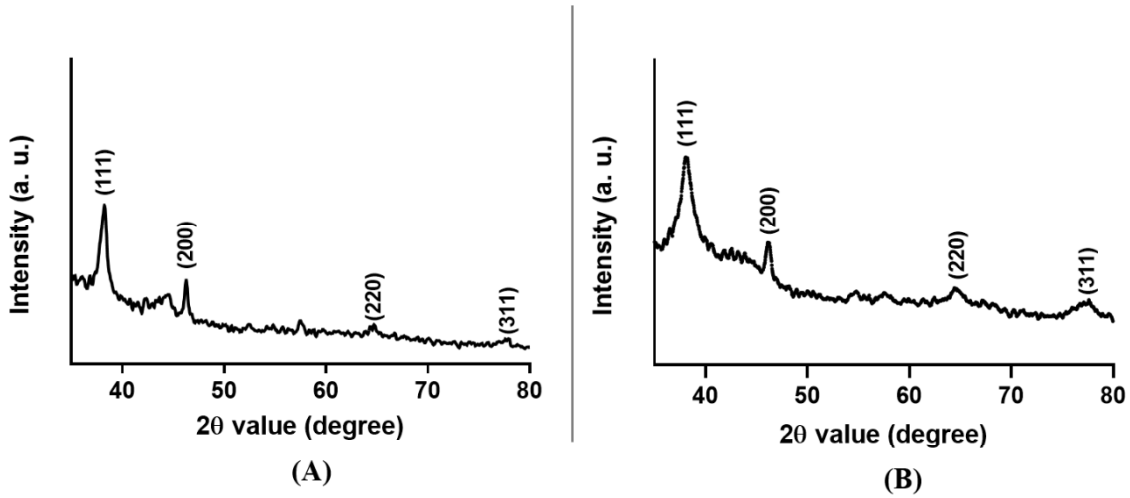

Figure 2.15: XRD spectra of Ag NPs synthesized by (A) *Penicillium shearii* AJP05 and (B) *Penicillium janthinellum* DJP06, with Bragg's diffraction values shown in parentheses.

XRD measurement of drop coated Ag NPs synthesized by both the fungal species showed well-defined peaks at the 2θ value of 37.96°, 46.26°, 64.31° and 77.30°, which were annotated to (111), (200), (220) and (311) planes of silver, respectively, as per JCPDS file no. 04-0783 (Figure 2.15). The obtained Bragg's diffraction values exhibited face-centered cubic structure of crystalline silver. Previous studies also showed similar diffraction pattern for Ag NPs (Jain et al., 2015; Gharpure et al., 2019).

Ag NPs synthesized by both the fungal species showed presence of negative charge on their surface with zeta potential values of -13.7 ± 0.4 and -21.5 ± 1.5 mV for *Penicillium shearii* AJP05 and *Penicillium janthinellum* DJP06, respectively. The obtained results suggest the capping of negatively charged proteins on the surface of Ag NPs.

FTIR measurements were performed to check the nature of capping materials present on the surface of as-synthesized Ag NPs. The obtained FTIR spectrums showed characteristic infrared bands at wave numbers 1637 and 3268 cm^{-1} in case of *Penicillium shearii* AJP05 and at wave numbers 1635 and 3384 cm^{-1} for *Penicillium janthinellum* DJP06. Wave numbers 1637/1635 cm^{-1} and 3268/3384 cm^{-1} correspond to the stretching vibrations of amide I and OH bonds, respectively (Figure 2.16). These results suggested the presence of fungal extracellular proteins as capping materials on the surface of Ag NPs. The obtained results are in alignment with previous reports (Fageria et al., 2017; Singh et al., 2018).

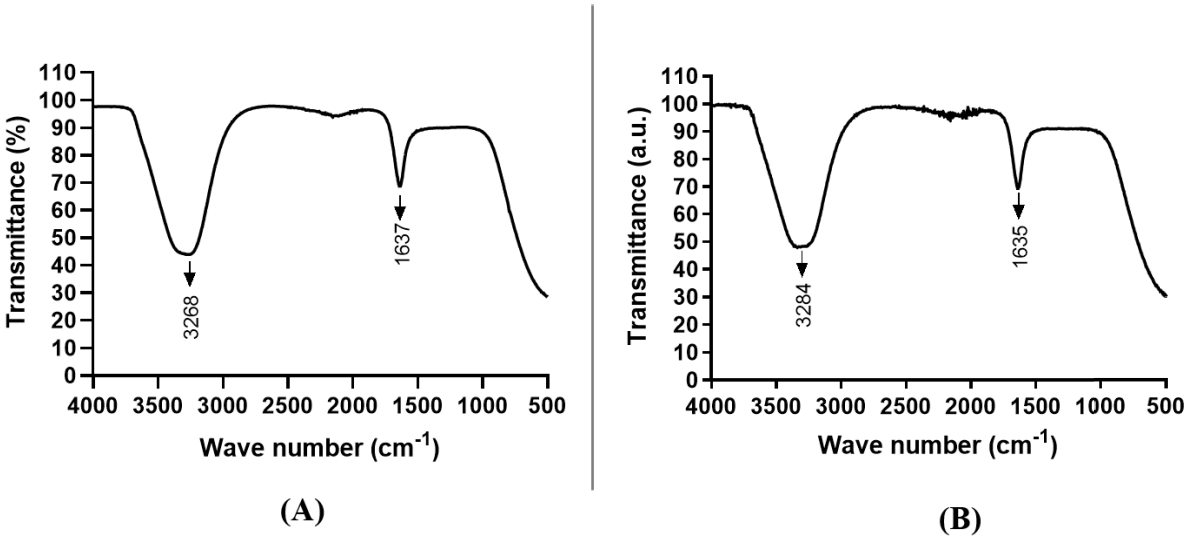

Figure 2.16: FTIR spectra of Ag NPs synthesized by (A) *Penicillium shearii* AJP05, and (B) *Penicillium janthinellum* DJP06.

2.4 Conclusion

In the present work, chemical and biological synthesis methods were used to synthesize Ag NPs with variation in their size and surface capping. Particles with an average size of 5, 10, 20, and 50 nm were synthesized and characterized to confirm their size, crystallinity and surface capping. Ag NPs of all the sizes were screened for their antibacterial potential against *Escherichia coli* K12 and based on the best antibacterial activity (discussed in Chapter 3), NPs of smaller size range (5-20 nm) were selected to study the effect of various surface coating

agents. Citrate, fucose and lysozyme were used to coat the chemically synthesized Ag NPs as a chemical agent, sugar and commercial protein, respectively. Whereas, the Ag NPs synthesized using fungi namely *Penicillium shearii* AJP05 and *Penicillium janthinellum* DJP06, were capped with fungal proteins. The myco-synthesized Ag NPs were found to have quasi-spherical shape, round edges and crystalline nature. The chemically and biologically synthesized particles with varying physico-chemical properties (size and surface capping) were further used to check their antibacterial potential.